

Dear Author,

Please correct your galley proofs carefully and return them no more than four days after the page proofs have been received.

Please limit corrections to errors already in the text; cost incurred for any further changes or additions will be charged to the author, unless such changes have been agreed upon by the editor.

The editors reserve the right to publish your article without your corrections if the proofs do not arrive in time.

Note that the author is liable for damages arising from incorrect statements, including misprints.

Please note any queries that require your attention. These are indicated with a Q in the PDF and a question at the end of the document.

Reprints may be ordered by filling out the accompanying form.

Return the reprint order form by fax or by e-mail with the corrected proofs, to Wiley-VCH : advmattechnol@wiley.com

To avoid commonly occurring errors, **please ensure that the following important items are correct** in your proofs (please note that once your article is published online, no further corrections can be made):

- **Names** of all authors present and spelled correctly
- **Titles** of authors correct (Prof. or Dr. only: please note, Prof. Dr. is not used in the journals)
- **Addresses** and **postcodes** correct
- **E-mail address** of corresponding author correct (current email address)
- **Funding bodies** included and grant numbers accurate
- **Title** of article OK
- All **figures** included
- **Equations** correct (symbols and sub/superscripts)

Corrections should be made directly in the PDF file using the PDF annotation tools. If you have questions about this, please contact the editorial office. The corrected PDF and any accompanying files should be uploaded to the journal's Editorial Manager site.

Author Query Form

WILEY

Journal ADMT
Article admt202100551


Dear Author,

During the copyediting of your manuscript the following queries arose.

Please refer to the query reference callout numbers in the page proofs and respond.

Please remember illegible or unclear comments and corrections may delay publication.

Many thanks for your assistance.

Query No.	Description	Remarks
Q-license	Please note that the article can only be published once an appropriate license agreement has been signed. The responsible corresponding author will have received an e-mail invitation to register/log in and sign a license agreement in Wiley Author Services (https://authorservices.wiley.com). The costs of publishing this manuscript OnlineOpen might be covered by one of Wiley's national agreements. To find out more please visit, https://authorservices.wiley.com/authorresources/Journal-Authors/open-access/affiliation-policies-payments/index.html . Eligibility for fee coverage is determined by the affiliation of the responsible corresponding author.	✓
Q1	Please confirm that forenames/given names (blue) and surnames/family names (vermilion) have been identified correctly.	✓
Q2	Please check the citation of 2b here for correctness.	✓
Q3	Please provide the volume number for ref. (40).	 111

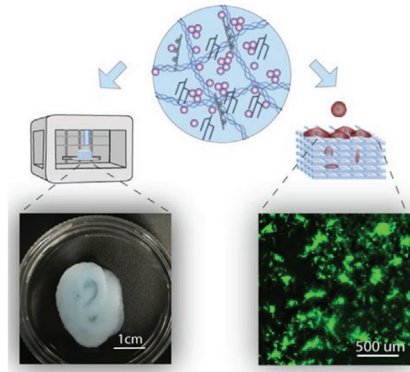
Please confirm that Funding Information has been identified correctly.

Please confirm that the funding sponsor list below was correctly extracted from your article: that it includes all funders and that the text has been matched to the correct FundRef Registry organization names. If a name was not found in the FundRef registry, it may not be the canonical name form, it may be a program name rather than an organization name, or it may be an organization not yet included in FundRef Registry. If you know of another name form or a parent organization name for a "not found" item on this list below, please share that information.

FundRef Name	FundRef Organization Name
NIH NIGMS MIRA	✓

P. Zhuang, Z. Greenberg,
M. He*.....2100551

**Biologically Enhanced Starch Bio-Ink
for Promoting 3D Cell Growth**



To fulfill the physiochemical requirement of bioprinting and support the cell growth, a novel, printable and shear-thinning nanocomposite starch-based hydrogel is formulated. The developed starch-based nanocomposite hydrogel is mechanically competent to maintain superior printability and shape fidelity while sustaining long-term cell growth, facilitate cell attachment, migration, and proliferation.

Biologically Enhanced Starch Bio-Ink for Promoting 3D Cell Growth

Pei Zhuang, Zachary Greenberg, and Mei He*

The excellent rheological property has legitimated the suitability of starch hydrogel for extrusion-based 3D printing. However, the inability to promote cell attachment and migration has precluded the non-modified starch hydrogel from direct applications in the biomedical field. Herein, a novel 3D printable nanocomposite starch hydrogel is developed with highly enhanced biocompatibility for promoting 3D cell growth, by formulating with gelatin nanoparticles and collagen. The rheological evaluation reveals the shear-thinning and thixotropic properties of the starch-based hydrogel, as well as the combinatorial effect of collagen and gelatin nanoparticles on maintaining printability and 3D shape fidelity. The homogeneous microporous structure with abundant collagen fibers and gelatin nanoparticles interlace and supplies rich attachment sites for cell growth. Corroborated by the cell metabolic activity study, the multiplied proliferation rate of cells on the 3D printed nanocomposite starch hydrogel scaffold confirms the remarkable enhancement of biological function of the developed starch hydrogel. Hence, the developed nanocomposite starch hydrogel serves as a highly desirable bio-ink for advancing 3D tissue engineering.

1. Introduction

3D bioprinting offers an unmatched potentiality for creating stand-alone and well-defined tissue architectures with either intricate patterns or customized zones.^[1–3] 3D printed scaffold can greatly improve the mass transport throughout the cultured tissue system, which is highly attractive for various tissue engineering applications. One of the determining factors for successful printing is from bio-ink^[6,7] which ideally fulfills the requirements of the adopted printing technique, for instance, viscosity, shear-thinning, low yield stress, and thixotropic property, but, of the utmost importance, supporting the attachment and 3D growth of seeded cells.^[8,9]

Natural extracellular matrix (ECM) biomaterials, such as collagen, undergo irreversible deformation when extruded after gelation without the ability to retain the material shear thinning. Most importantly, the natural ECM materials such

as collagen have low stiffness, which significantly limits the ability to form free-standing structures for maintaining good 3D shape fidelity.^[10] Modifications such as the addition of various rheological modifiers and postprinting or on-site chemical/photo-crosslinking have been employed, which resulted in an increasing diversity of mechanically competent materials for 3D bioprinting.^[11,12] However, such crosslinking steps could impair the biocompatibility of developed 3D bio-ink by introducing exogenous chemical groups subjecting to potential toxicity and immunogenicity in both *in vitro* and *in vivo* applications, or resulting in a mechanically incoherent network that impedes the desired cellular responses. Given the requirement of both desired mechanical property and biological function, using naturally derived biomaterials without any chemical modification for 3D printing is critically challenging.^[13]

Owing to its cost-effectiveness, availability, biocompatibility, and excellent biodegradability under physiological conditions, starch has been identified to be an appealing natural biomaterial for tissue regeneration and drug delivery.^[14,15] In order to improve cell adhesion ability and thermal stability from starch, other polymers such as PVA, chitosan, and collagen have been introduced to form starch-based blends.^[16–18] Through physically associated networks, starch-based blends with improved mechanical strength, biocompatibility, and processability have been achieved. Early studies have demonstrated the utility of starch-based scaffolds for bone tissue engineering.^[19,20] Recent years have witnessed an increasing exploration of the therapeutic potential in wound healing of starch-based scaffolds.^[21,22] Various types of starch have been tailored into scaffolding preparation methods such as electrospinning, salt leaching, injection molding.^[18,23,24] To expand its versatility, recent studies have also demonstrated the suitability of starch hydrogel for 3D bioprinting.^[14] However, the reported studies either utilize starch with a higher concentration over 25% to secure the mechanical stiffness, or sacrifice 3D printability of starch in the low concentration range.^[25]

In order to overcome above-mentioned limitations, we introduce a novel 3D printable nanocomposite starch hydrogel with highly enhanced biocompatibility for promoting 3D cell growth, by formulating with natural collagen and gelatin nanoparticles. Although a wide series of nanoparticles, including nanosilicates,^[26,27] starch or cellulose nanocrystals,^[12,28] gold

P. Zhuang, Z. Greenberg, M. He
Department of Pharmaceutics
University of Florida
2033 Mowry Rd, Gainesville, FL 32608, USA
E-mail: mhe@cop.ufl.edu

The ORCID identification number(s) for the author(s) of this article can be found under <https://doi.org/10.1002/admt.202100551>.

DOI: 10.1002/admt.202100551

nanoparticles,^[29] carbon nanotube, and graphene oxide have been investigated and incorporated into hydrogel networks to achieve desired material properties (e.g., electrical conductivity, printability, mechanical stiffness, and stimuli response),^[30,31] using gelatin nanoparticles in starch hydrogel for enhancing 3D cell culture and tissue scaffolding ability has not been explored elsewhere. With the incorporation of gelatin nanoparticles and collagen in starch-based hydrogel to bring nanoscale topological features, cells could reside in a highly biocompatible microenvironment for interactive binding and attachment, which is critically needed in regulating 3D cellular response and tissue growth. We optimized the composition of developed starch hydrogel for achieving the high 3D printing fidelity through dynamic rheological characterization and printability evaluation. The results demonstrated that the combination of gelatin nanoparticles and collagen could tune the mechanical stiffness as desired for extrusion-based 3D bioprinting. Further microstructure analysis revealed that the nanocomposite hydrogel encompassed hierarchical porous structures with distinct fibrous collagen distributing throughout the pore surface, which is highly desirable for cell attachment and migration. In vitro cellular response investigation using mammalian fibroblasts showed excellent cellular viability and interaction with 3D printed nanocomposite starch hydrogel. Therefore, this work introduces a non-modified, low-cost, and handy 3D printable nanocomposite starch hydrogel, with complementary network formed by gelatin nanoparticles and collagen for enhancing its biological property. We expect this highly biocompatible 3D printable nanocomposite starch bio-ink could be broadly employed in the field of 3D tissue engineering and therapeutic development.

2. Results and Discussion

2.1. Evaluations of GNPs

Gelatin nanoparticles were synthesized successfully based on a two-step coagulation process.^[32] NTA and DLS analysis were both employed to determine the size of GNPs, as revealed in Figure 1a and Figure S1 (Supporting Information). We observed the peak size of GNPs at ≈ 40 nm (diameter), from NTA analysis,

which is consistent with the observation from SEM imaging (Figure 1b). Although the results from DLS showed a broader distribution and a peak particle size at ≈ 106 nm (diameter), due to the recognition of the scattering intensity fluctuation from the DLS, the contribution from the smaller particles could be overshadowed by the higher scattering signals from the larger particle aggregates, leading to the overshooting on the nanoparticle size. The cytotoxicity of the GNPs was evaluated using PrestoBlue assay that relies on metabolic activity of the active NIH 3T3 cells. Gelatin nanoparticles with varied concentrations spanning from 0 to 10^{10} particles mL^{-1} were incubated with NIH 3T3 cells for 5 d. As evidenced in Figure 1c, the cell proliferation rates in the groups with GNPs were comparable to the non-GNPs control group, highlighting the negligible toxicity of GNPs on cultured cells.

2.2. Preparation of GNP Nanocomposite Starch Bio-Ink

Starch, as the plant-derived polysaccharide, has been recognized as a natural material in the field of tissue engineering due to its biocompatibility, biodegradability, and ultralow cost. The property of starch is generally governed by the ratio of two main structural components: amylose and amylopectin.^[33] The amylose impairs the gel strength, while the amylopectin determines the gel viscosity. The formation of starch hydrogel is a three-step thermal treatment that includes swelling, gelatinization, and retrogradation to form a 3D hydrogel network (Figure S2 and 2b, Supporting Information).^[34] To introduce the GNPs into the starch hydrogel, we first suspended the GNPs with the desired concentration into 50 mmol HEPES buffer, then vigorously mixed with starch granules for 20 min to form the GNP-supplemented starch hydrogel (Figure 2a). Additionally, we added collagen as a cell-instructive component to mimic the native tissue due to its ubiquitous presence in most tissues and organs. Collagen forms fibrous networks in the body, which can enhance the tissue structure and function of ECM while promoting cell adhesion, growth, tissue morphogenesis, and biological signaling. We have investigated six combinations of starch, collagen, and GNPs for developing the best 3D bio-ink recipe in terms of printing fidelity, structural integrity, and cell growth. The 3D printed anatomical ear structure was shown as

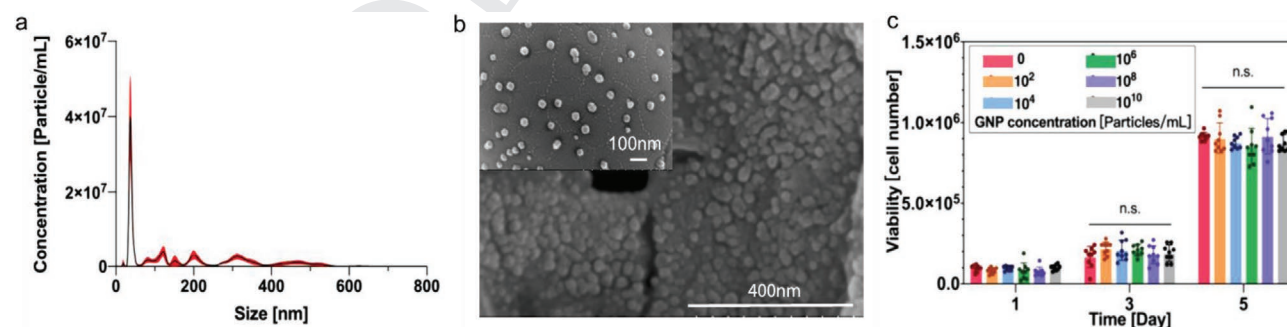


Figure 1. Assessment of gelatin nanoparticles (GNPs) in terms of size distribution, morphology, and toxicity on cell proliferation. a) Size and concentration measurement using Nanoparticle tracking analysis (NTA). Red color indicates the standard deviation. b) FESEM images of gelatin nanoparticles in DI water with lower and higher magnifications (insert). c) Effects of GNP concentration on the cell proliferation over a 5 d culture ($n = 9$ technical replicates), determined using a Prestoblue assay.

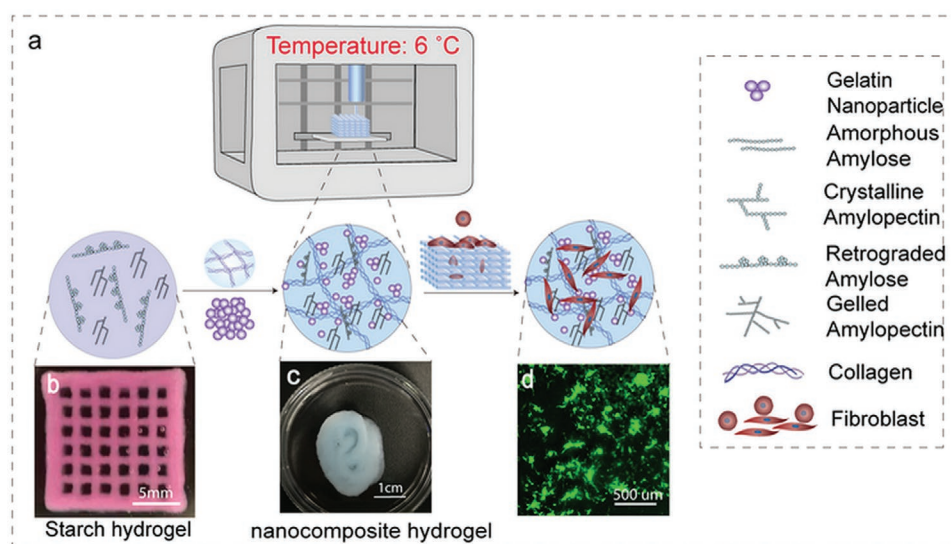


Figure 2. a) Schematic illustration of the development of 3D printable nanocomposite starch-based hydrogel b) The insert image showed the grid pattern in good shape fidelity with 15 mm × 15 mm × 2 mm cubic structure that can be 3D printed with pure starch hydrogel. c) 3D Printed anatomical ear using nanocomposite starch-based hydrogel with good shape fidelity. Printing temperature was maintained at 6 °C. Blue color is food dye. d) NIH 3T3 cell spreading on 3D printed nanocomposite starch hydrogel scaffold over a 7 d culture, indicating the excellent ability for promoting cell growth and attachment.

the example in Figure 2c demonstrating the excellent printing fidelity. The printed scaffold also exhibits improved biological property to promote cell attachment and proliferation, as shown in Figure 2d by culturing NIH 3T3 cells for 7 d.

2.3. Rheological Characterization of Nanocomposite Starch-Based Hydrogels

We investigated the rheological profiles of variable combinations of GNPs, starch hydrogel, and collagen, which could inform the development of high-quality bio-ink with the best printability and the 3D shape fidelity. As demonstrated in Figure S6 (Supporting Information) by printing a 10-layer scaffold in a grid pattern, we observed that starch is the dominant factor to maintain the 3D printability, as long as the concentration is larger than 10%. The addition of collagen had adversely affected the printability. This observation was further quantitatively validated by

shear rate sweep analysis in Figure 3a, along with the pure starch hydrogels and starch-collagen blend as the control group. As confirmed, a significant increase in viscosity was observed along with increasing starch concentration across all the groups. Interestingly, the addition of collagen resulted in the 90.52%, 61.51%, 38.91% reduction of zero-shear viscosity, compared to the corresponding groups with 7.5%, 10%, and 12.5% pure starch hydrogel only. The final concentration of collagen at 1.33 mg mL⁻¹ in the hydrogel system exhibits extremely low viscosity (≈5.3 mPa s) which is close to water viscosity at low temperature, thus, leading to the reduced viscosity due to the dilution of the entire hydrogel system.^[35] However, along with the increased starch concentration overpowering the influence on the overall material, the collagen influence on viscosity reduction of the overall material is minimized. The

incorporation of GNPs has enhanced the viscosity of starch-collagen blend in a concentration-dependent manner, as shown in Figure S3 (Supporting Information). With a GNP concentration of 1×10^{10} particles mL⁻¹, the formed nanocomposite starch-collagen hydrogel exhibits reinforced viscosity, which is comparable to the pure starch but with significantly enhanced cellular interaction sites introduced by collagen material.

Frequency sweep offers a well-defined comparison of viscoelastic properties under constant strain. As illustrated in Figure 3b, the storage modulus G' is larger than the loss modulus G''

under the applied angular frequency in the entire frequency region for all the groups. Additionally, both G' and G'' increased with increasing angular frequency. Although no cross-over point appeared in any group, G'' and G' of samples with a starch concentration at 7.5% and 10% are converging at higher values of ω . This result implies the gradual loss in the elastic property in the tested gel-like materials. Overall, frequency sweep analysis cooperatively confirmed the significance of starch in maintaining the mechanical property of all the tested groups, as well as the beneficial effect from the collaboration of collagen and gelatin nanoparticles on manipulating the viscosity and mechanical strength of nanocomposite hydrogel, making it tunable to specific applications.

Thixotropy is a time-dependent shear-thinning behavior that is considered to be associated with the rheological instability of a material. By applying a certain shear rate, the weak physical bonds are mechanically disrupted, and the inner structures disintegrate to separate from aggregates. Such process is shear rate- and time-dependent. Therefore, thixotropy plays a pivotal role in determining the shape fidelity of the 3D-printed constructs. In this study, the thixotropic properties of the nanocomposite hydrogel samples were investigated through a three-phase measurement as shown in Figure 3c.

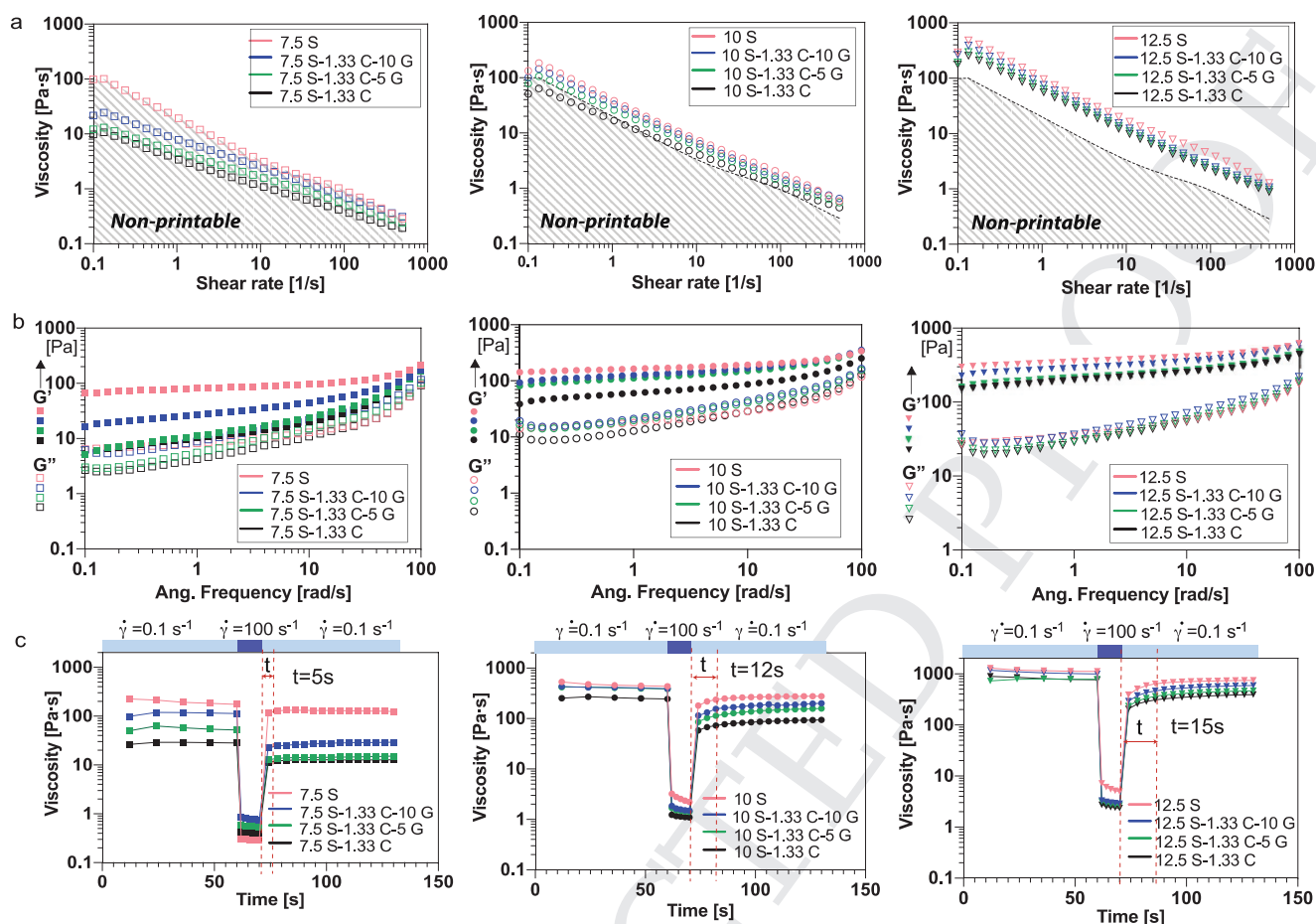


Figure 3. Rheological characterization of starch, the starch-collagen blend, and nanocomposite starch-based hydrogel during the extrusion condition at 6 °C a) Shear rate sweep analysis of starch, the starch-collagen blend, and nanocomposite starch-based hydrogel. b) Frequency sweep indicates G' (closed symbol) and G'' (open symbol) profiles of starch, the starch-collagen blend, and nanocomposite starch-based hydrogel at varied concentrations. c) Representative recovery performance and thixotropy profiles from tested material groups. (S: starch, C: collagen, G: gelatin nanoparticles. Number in front of each letter indicates the final concentration of each component. Starch concentration: 7.5%, 10%, 12.5% w/v; Collagen: 1.33 mg mL⁻¹; Gelatin nanoparticle: 5G: 3.33×10^9 and 10G: 6.67×10^9 particles mL⁻¹).

At a given concentration of starch, starch-collagen blend, and the nanocomposite hydrogels all showed the similar recovery trend, in terms of time to reach equilibrium. An increased starch concentration could yield a longer recovery time. With a starch concentration at 10% and 12.5%, introducing GNPs significantly improved the recovery performance in comparison to the starch-collagen blend only, which led to a comparable recovery rate as the pure starch hydrogel. It is worth noting that the dissolving of starch granules could be incomplete at room temperature. The presence of the swollen but non-melted starch granules could cause a retarded and incomplete recovery. In this study, we formed starch hydrogel at 45 °C. Despite the relatively slow recovery, the nanocomposite starch hydrogel showed the shear-thinning and thixotropic property, which is highly desired for extrusion-based 3D bioprinting.

2.4. Printability and the Structural Integrity

When creating a 3D bioprinted construct, one of the most important considerations is the ability to maintain the desired

shape during and after printing. The desired outcome from extruded material is to retain constant width and smooth edges in the shape of the extrusion path without bulging, thinning or breaking. As reported in the previous study, the printability of the materials could be quantitatively investigated using Equation (1).^[36]

$$\text{Pr} = \frac{\pi}{4} \cdot \frac{1}{C}, \text{ where } C = \frac{4\pi A}{L^2} \quad (1)$$

L is the perimeter of the enclosed area (labeled with red dash line in Figure S7, Supporting Information), and A is the area. Therefore, for a square, $C = \frac{\pi}{4}$; while for a circle, $C = 1$. Correspondingly, the Pr for a square is 1, and for a circle is $\frac{\pi}{4}$. The larger the Pr value is, the better the printability is, which may indicate the less impairment on printing resolution and 3D stacking from reduced material viscosity and gelation degree. For an ideal gelation condition or perfect printability status, the interconnected channels of the constructs would demonstrate a square shape, and the Pr value is 1. From our study in Figure S6

(Supporting Information), Pr value larger than 0.8 could show acceptable printability. From published literature, Pr value within the range of 0.9–1.1 demonstrated satisfied filament morphology and mechanical stability of the printed construct.^[37,38] The printability of the formulated hydrogels with the starch concentration at 12.5% was calculated, as shown in Figure 4a and Figure S7 (Supporting Information). Starch-collagen blends showed the circular enclosed area between the printed filaments, and thus a relatively lower Pr value (0.857 ± 0.008). Pure starch has the highest Pr value at 0.929 ± 0.032 and the thinnest filaments (as displayed in Table S1, Supporting Information), demonstrating the superior 3D printability. Enhanced shape fidelity was observed with the supplement of GNPs, which is in good alignment with the rheological investigation in Figure 3.

In addition to the 3D printability, the structural integrity and stability during the culture process are also crucial. Figure 4b shows the representative images of all the tested material samples over a 14 d immersion in PBS. The 3D constructs from the pure 12.5% starch hydrogel were corrupted and dispersed within 24 h of culture, which could be due to the incomplete gelatinization of starch granules. In contrast, other biomaterial samples blended with collagen and GNPs maintained a stable 3D structure. With the thermo-gelation of collagen taking place during the culture, the 3D constructs could further be stabilized for supporting long-term 3D cell culture and tissue growth.

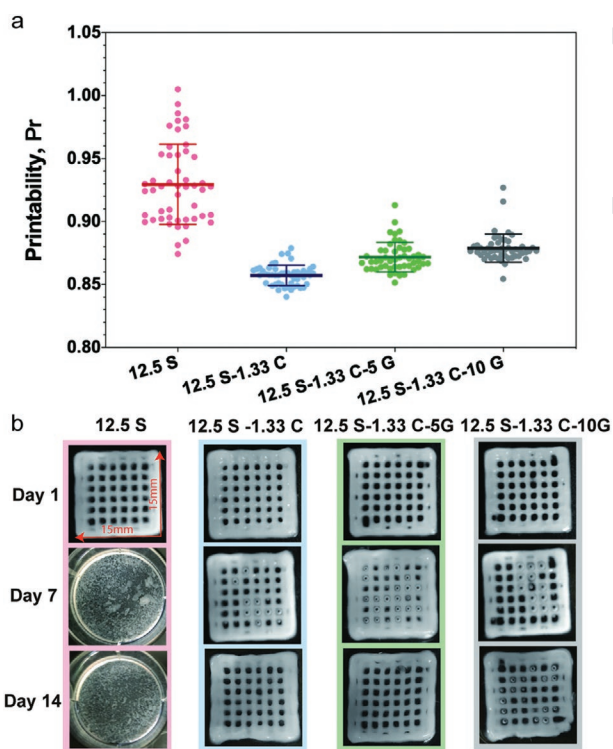


Figure 4. a) Characterization of the printability of starch, the starch-collagen blend, and the nanocomposite starch hydrogel ($n = 6$). b) The structural integrity of 3D printed hydrogels in PBS over a 14 d incubation ($n = 6$). (S: starch, C: collagen, G: gelatin nanoparticles. Number in front of each letter indicates the final concentration of each component. Starch concentration: 12.5% w/v; Collagen: 1.33 mg mL^{-1} ; Gelatin nanoparticle: 5G: 3.33×10^9 and 10G: 6.67×10^9 particles mL^{-1}).

2.5. Morphological Microstructure Characterization

The porosity plays a pivotal role in scaffolding biomaterials, which can facilitate mass transport associated nutrient and biological exchange for promoting 3D cell growth. We examined the microstructure of the starch, starch-collagen blend, and nanocomposite starch hydrogel using a cryo-scanning electron microscope (Cryo-SEM). ImageJ was used to analyze the Cryo-SEM images to determine the pore size distribution, porosity, and wall thickness within the hydrogel matrix. With a fixed starch concentration at 12.5%, we observed interconnected hierarchical porous structures in all the tested material samples (Figure 5 and Figure S4, Supporting Information). This honeycomb-like porous structure implied the capacity to facilitate cell migration, proliferation, oxygen, and nutrient transport, as well as the potential applications for drug loading and release in void space.

The pure starch hydrogel possesses a smooth surface and relatively thin walls throughout the entire matrix, along with a few starch fibers stretching out from the surface (Figure 5a). However, by adding collagen as the blend (Figure 5b,c), we observed a significantly heterogeneous pore surface, with much larger hierarchical pores. The collagen fibers are readily identifiable and randomly stretching out of starch for supplying rich binding sites to promote cellular attachment. Notably, the addition of collagen can enlarge the matrix pore size, as well as thicken the wall of hydrogel. As evidenced in Figure 5j,m, both the pore size and wall thickness from the starch-collagen blend are nearly twofold higher than that from the pure starch hydrogel. Notably, by further incorporating GNPs into the starch-collagen blend, we observed a higher order of homogeneous microporous structure and abundant collagen fibers, although with the entire hydrogel network compacted in a smaller pore size (Figure 5e,k, and Figure S4, Supporting Information). We suspect that GNPs can induce denser hydrogel network to reinforce the scaffolding mechanical strength, which is also supported by our rheological study in Figure 3. The loaded GNPs were found to be merged with the skeleton of the matrix (Figure 5h), as well as attaching to collagen fibers for forming an interlaced web-like structure (Figure 5f,g red arrows). The histogram of pore size distribution and porosity of all three samples were displayed in Figure 5i-k. Compared with the starch or starch-collagen hydrogels, by introducing the GNPs, the material pore structures are denser to reinforce the overall mechanical stiffness of nanocomposite hydrogel.

2.6. In Vitro Cell Culture on 3D Printed Nanocomposite Starch-Based Hydrogel Scaffold

Current starch hydrogel has been widely used as 3D bio-ink in tissue engineering yet, due to its inability for cell adhesion and migration and thermal instability during the culture period. To further evaluate the potential of the developed nanocomposite starch-based hydrogel for serving as ideal bio-ink in tissue engineering, NIH 3T3 fibroblasts were seeded on the top of the 3D printed nanocomposite starch hydrogel in a grid pattern. As mentioned above, pure starch scaffolds were not suited for tissue culture due to their instability and rapid collapse

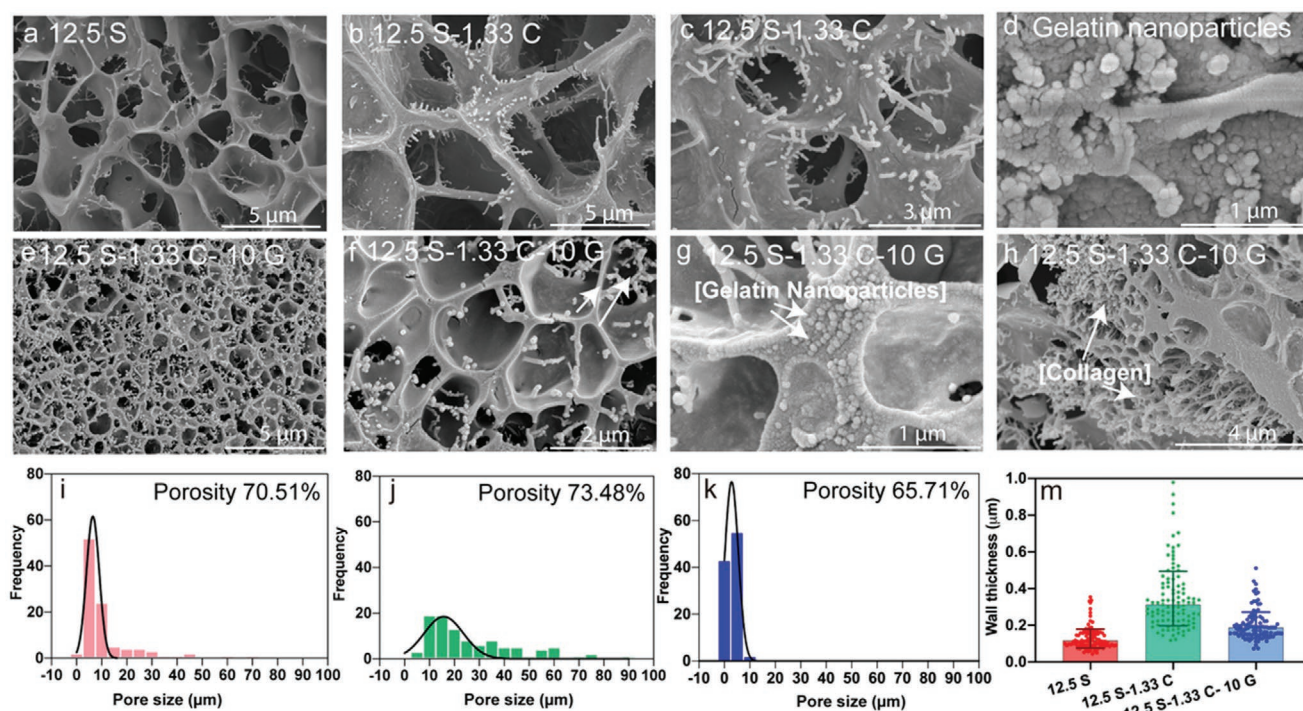


Figure 5. Cryo-SEM images present the hierarchical porous microstructures from a) pure starch, and hybridized hierarchical pores and fibrous sprouts from the starch–collagen blend in b) and c). d) The SEM image showing the gelatin nanoparticles in HEPES buffer around 40 nm in size. The unique hydrogel network reinforced by GNPs with interlaced web-like structures was shown by Cryo-SEM imaging in different scales at e) 5 μm, f) 2 μm, g) 1 μm, and h) 4 μm. The pore size distribution and porosity from i) starch, j) starch–collagen blend, k) nanocomposite starch hydrogel were characterized using ImageJ analysis of Cryo-SEM images. m) The scaffold wall thickness from all three samples ($n = 100$). (S: starch, C: collagen, G: gelatin nanoparticles. Number in front of each letter indicates the final concentration of each component. Starch concentration: 12.5% w/w; Collagen: 1.33 mg mL⁻¹; Gelatin nanoparticle: 10G: 6.67×10^9 particles mL⁻¹).

during culture conditions. Here we used a 3D printed starch–collagen blend as a control group for 3D cell culture. Figure S5 (Supporting Information) showed the cell distribution after seeding for 3 h at day 1 with consistent seeding density across all samples (seeding density $\approx 10^6$ cells mL⁻¹). The majority of the cells were resting in the cavity of the printed grid pattern. During culture, cells grow and start to attach, spread, and migrate on the surface of the scaffolds. As shown in Figure 6, on day 4, cells seeded on the material of starch–collagen–nanoparticle hydrogel exhibited excellent attachment and migration. In contrast, cells on the starch–collagen hydrogel mainly stayed at the interconnected channels, and only a few cells were observed on the edge of the scaffold, indicating limited migration. On day 7, as illustrated in Figure 6i,j, the attached cells further stretched and elongated on the scaffold of starch–collagen–nanoparticle hydrogel and achieved better uniformity distribution on the nanocomposite scaffold with network formation (Figure 6f,h), while cells on starch–collagen scaffold showed poor migration (Figure 6b,d). Figure 6i,j gave a better view of comparison to the control group, regarding cell distribution, stretch, and elongation within our developed nanocomposite starch-based hydrogel. The cell metabolic activity analysis in Figure 6k quantitatively demonstrated a much faster cell proliferation rate with nearly twofold enhancement in our developed nanocomposite starch hydrogel. Collectively, the results highlighted the enhancement on cell attachment, elongation, and migration by using a developed material blend,

which could be ideal 3D tissue scaffolding for improving 3D cell growth.

3. Conclusions

Starch is an appealing natural biopolymer for versatile tissue engineering applications, owing to its cost-effectiveness, scalable production, biocompatibility, and biodegradability. However, due to the mechanical instability and the absence of cell-binding sites, starch has not been widely used as the 3D bio-ink in the field of tissue scaffolding. In this work, we present a novel formulation of 3D printable starch-based hydrogel with desired biological property and improved stability by blending starch with collagen as well as the gelatin nanoparticles. Through the rheological characterization, this novel nanocomposite starch hydrogel exhibits highly desired shear-thinning and thixotropic property, as well as the mechanical strength suited in high-fidelity 3D printing. Gelatin nanoparticles also functioned as a rheological modifier, which can tune the mechanical strength over a wide range for tailoring to variable tissue engineering applications. By formulating starch with gelatin nanoparticles, the resulted bio-ink showed significantly enhanced mechanical property and enabled the preservation of shape fidelity, which compensated the loss of mechanical strength when blended with collagen. The unique homogeneous microporous structure with abundant collagen

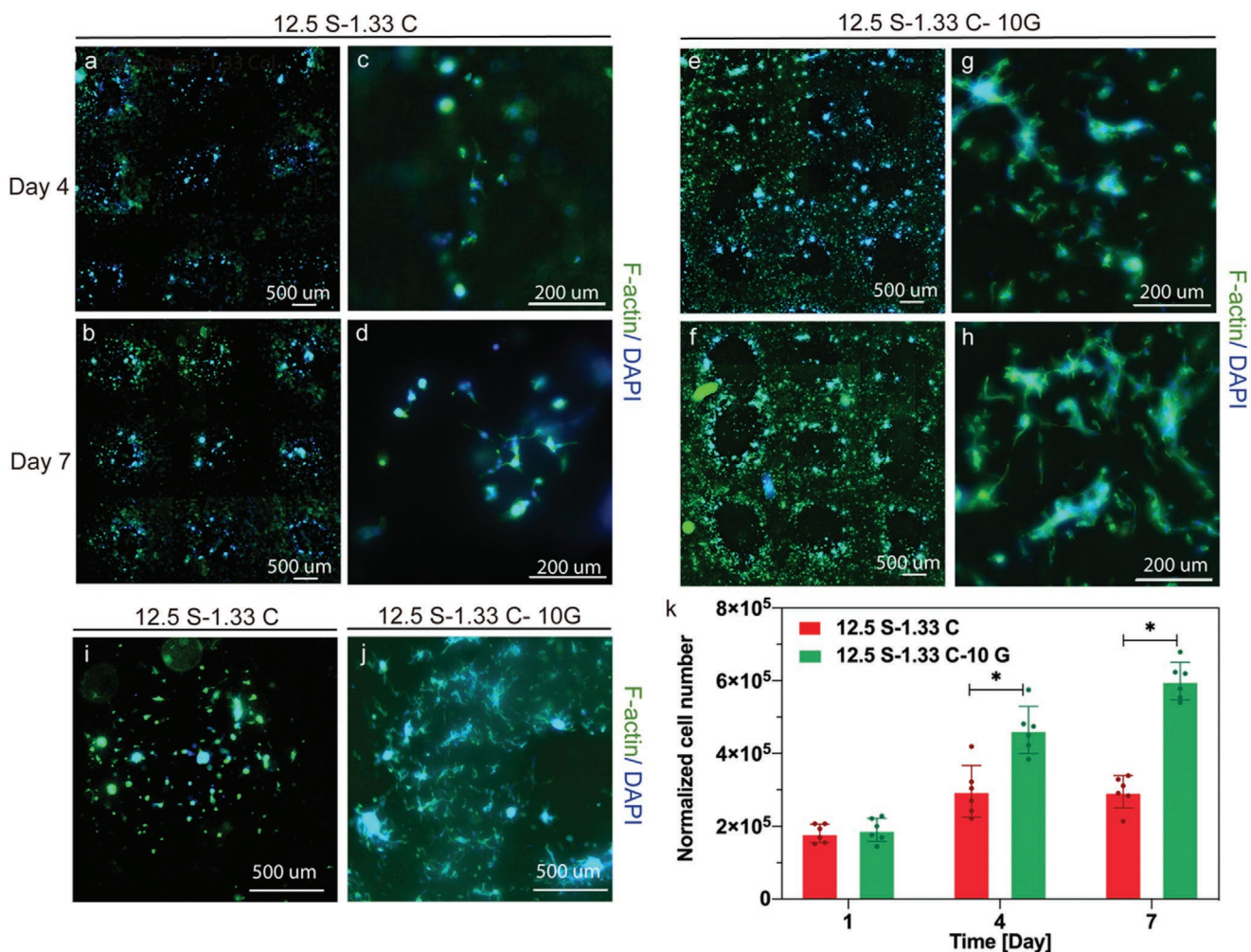


Figure 6. Evaluation of cellular response on 3D printed nanocomposite starch-based hydrogel scaffold Starch-collagen blend hydrogel scaffold serves as the control group. Limited cell growth on starch-collagen blend hydrogel scaffold on a,c) Day 4 and b,d,i) Day 7, compared with abundant cell attachment and spreading on 3D printed nanocomposite starch bio-ink on e,g) Day 4 and f,h,i) Day 7. k) Evaluation of cell proliferation on both scaffolds over a 7 d culture ($n = 6$). (S: starch, C: collagen, G: gelatin nanoparticles. Number in front of each letter indicates the final concentration of each component. Starch concentration: 12.5% w/v; Collagen: 1.33 mg mL⁻¹; Gelatin nanoparticle: 10G: 6.67×10^9 particles mL⁻¹).

fibers and GNP interlaced web-like structure not only support the efficient mass transport, but also supplies rich attachment sites for promoting 3D cell growth, as evidenced by culturing fibroblast cells with fold increased proliferation rate. Due to the enhanced mechanical strength, the developed starch nanocomposite hydrogel scaffolds are able to maintain good 3D structural integrity with reduced degradation rate for being gradually replaced along with cell growing, and remodeled to match the complexity of real tissue microenvironment, which is critically needed for long-term tissue culture.

Although there are many scaffold biomaterials developed in the field of tissue engineering and regenerative medicine, current clinical translation is still hampered due to the concerns from the toxicity and biocompatibility. The chemical and mechanical properties of the biomaterial scaffold must be optimized to suit the interaction with cells and the surrounding tissue microenvironment, including the efficient mass transport and host tissue integration. Our developed nanocomposite starch bio-ink has the ability to tune the mechanical strength

by varying the concentration of each component, which offers a great opportunity to tailor to the specific tissue environment. Such flexibility also allows the potential for incorporating live cells during the 3D extrusion printing process which is undertaking in our research lab as one of the future directions. Additionally, the developed nanocomposite starch is completely non-toxic and non-chemically modified, therefore, the starch nanocomposite is still highly biodegradable via converting carbohydrates back into forms that are usable for various bio-synthetic and metabolic routes in vivo. We foresee this novel material platform holds great potential for clinical use and commercialization in regenerative medicine, as well as promoting biomimetic tissue engineering and research.

4. Experimental Section

Materials: Commercial pregelatinized native common corn starch (Cargill Gel-Instant 12030) was gratefully supplied by Cargill, USA. Ham's

F-12K medium, Dulbecco's phosphate buffered saline, heat-inactivated fetal bovine serum, penicillin/streptomycin, Cell Tracker Red CMTPX, LIVE/DEAD Viability/Cytotoxicity Kit, PrestoBlue Cell Viability Reagent, DAPI and Alexa Fluor 488 Phalloidin for cell culture and characterization were purchased from Thermo Fisher Scientific. Collagen type I from rat tail was purchased from Advanced BioMatrix, Carlsbad, CA (Catalog #5279). Type A gelatin from porcine skin (300 g Bloom), glycine, HEPES, and 25% glutaraldehyde solution were obtained from Sigma-Aldrich, USA. Other chemicals including acetone, sodium hydroxide, and hydrochloric acid (1N HCL solution) were purchased from Fisher Sci, USA.

Preparation of Gelatin Nanoparticles (GNPs): Gelatin nanoparticles were prepared by a two-step coagulation process based on a previously reported study.^[32,39] Briefly, 0.625 g gelatin was dissolved in 12.5 mL DI water at 40 °C under constant stirring for 1 h. 12.5 mL acetone was introduced to the solution at a syringe pump-driven constant speed 0.1 mL s⁻¹ under vigorous stirring (300 rpm). Thereafter, the solution was kept sitting for 15 min for the high molecular weight gelatin to precipitate, and the supernatant that containing low molecular weight gelatin was decanted. 7 mL DI water was subsequently added to redissolve the precipitated gelatin at 40 °C. Upon complete dissolution, the pH of solution was brought down to a range of 2.7–3.0 using hydrochloric acid. 16.5 mL acetone was further added to the solution at a rate of 1 mL min⁻¹ under constant stirring (600 rpm). 1 mL acetone containing 60 µL 25% glutaraldehyde solution was gradually fed to the solution at a rate of 0.05 mL min⁻¹ to crosslink the gelatin nanoparticles and the solution was stirred overnight. The reaction was deactivated by adding of 200 µL 1 M glycine solution. Acetone was then removed, and the solution was filtered through a 0.22 µm syringe filter. The achieved solution was stored at 4 °C for future use.

Nanoparticle Tracking Analysis: Gelatin nanoparticle's size distribution and concentration were determined by nanoparticle tracking analysis (NTA) using a NanoSight NS300 system (Malvern Technologies, Malvern, UK) configured with a 488 nm laser. Samples were diluted 50× in dPBS to an acceptable concentration. Samples were analyzed under constant flow conditions (flow rate = 50 µL min⁻¹) at 25 °C with a camera level of 8. Data were analyzed using NTA 3.4 software with a detection threshold of 5.

Dynamic Light Scattering: Dynamic light scattering allows for the characterization of particle size distributions with nanoparticles in various solutions through the analysis of the electrophoretic mobility. A Malvern Zetasizer (Malvern Panalytical Inc. 117 Flanders Road Westborough MA 01581-1042 United States) was used in conducting dynamic light scattering analysis of gelatin nanoparticles with a concentration of 10⁹ particles mL⁻¹ suspended in deionized water in 50-fold dilution. In preparing the sample for dynamic light scattering (Malvern Zetasizer), the scattering mode and angle were automatically selected as 90° inside scattering mode, with an equilibration time at 1 min and a temperature of 25 °C, before measuring five runs per sample. The sample was prepared in the pH 7.2 solution, with the wavelength of the incident laser at 633 nm. A cuvette loading cell was used and all results are listed with an average of five runs.

Scanning Electron Microscopy: Field emission -scanning electron microscopy (FE-SEM) was used for visualizing and probing the gelatin nanoparticles' morphology, topology, and size. Samples were first prepared through a serial dilution to a final concentration of 1 × 10⁹ particles mL⁻¹, followed with homogenization by light vortexing at 3000 rpm for 10 s, then directly aliquoted onto a 100% acetone-cleaned, Ted Pella aluminum pin stub mount (4595 Mountain Lakes Blvd, Redding, CA), and solution was allowed to evaporate completely. Immediately, the samples were sputter-coated for 60 s with an Au/Pd target using a Denton Desk V Sputter Coater (1259 North Church St. Bldg 3 Mooretown, NJ USA 08057), and loaded into the Hitachi SU5000 Schottky Field-Emission Scanning Electron Microscope (20770 W. Nordhoff Street, Building 4, Chatsworth, CA 91311, USA) at a high negative vacuum pressure of 10⁻⁸ torr. An incident electron beam was applied onto the samples at 7 keV and beam current of 16.7 nA. Aperture and stigmata corrections were done before sample images were obtained.

Cytotoxicity of GNPs: The cytotoxicity of GNPs was determined using PrestoBlue assay. Nanoparticles were suspended into culture medium to achieve final concentrations at 0, 10², 10⁴, 10⁶, 10⁸, 10¹⁰ particles mL⁻¹, respectively. Afterward, NIH-3T3 cells were plated at a density of 5 × 10⁴ cells per well in a 24-well plate for culturing with nanoparticle-loaded medium for 5 d. PrestoBlue reagent was added to the medium for a final concentration of 10% and incubated for 2 h at 37 °C. The absorbance was measured using Cytation 5, BioTek plate reader (λ = 570 nm). The intensity was then converted to cell numbers according to the plotted standard curve at each time point (1, 3, and 5d).

Preparation of Nanocomposite Starch-Collagen Hydrogel: The starch powder was sterilized by UV radiation thrice before use. The GNPs in DI water were loaded to HEPES buffer to achieve 50 mmol HEPES buffer (1 × PBS and pH = 7.4) containing a series of particle concentrations at 5 × 10⁹ and 10 × 10⁹ particles mL⁻¹. Starch was stirred into GNPs-containing HEPES buffer at 45 °C with constant stirring at 400 rpm for 20 min using an overhead mixer. After degassing by centrifugation for 30 min at 3000 × g, the GNPs-containing starch gels were kept in 4 °C fridge for 1 h. Prior to mixing, collagen was neutralized with HEPES buffer in 2× PBS in a 1:1 ratio.^[40,41] The buffer system was prepared by adding HEPES powder to PBS buffer to achieve a 50 × 10⁻³ M HEPES, pH = 7.4. Briefly, the HEPES buffer was prepared by adding HEPES powder into 2× PBS and was subsequently mix with collagen at concentrations of either 8 or 10.9 mg mL⁻¹ thoroughly to neutralize the collagen. The homogeneous nanoparticle/hydrogel composites were formed by mixing GNPs-loaded starch hydrogel and collagen through a three-way stop cock in a 2:1 ratio. Thus, nanoparticle/hydrogel composites with six different combinations (starch final concentrations at 7.5%, 10%, and 12.5% w/v; GNP final concentrations at 3.33 × 10⁹ and 6.67 × 10⁹ particles mL⁻¹; collagen at 1.33 mg mL⁻¹) were obtained (as shown in Table 1 with the labels of formulations used in the following experiments). The nanoparticle/hydrogel composites were kept in the fridge for 3 h before use. Starch gels at 7.5% w/v, 10% w/v, 12.5% w/v in HEPES buffer, and the starch-collagen hydrogel blends were prepared as the parallel control.

Rheological Evaluation: Rheological evaluation of the nanocomposite hydrogels was implemented on the MCR 702 MultiDrive rheometer (Anton Paar), using a 25 mm measuring plate. Strain sweeps, frequency sweeps, and shear rate sweeps were carried out at 6 °C. Strain sweeps in the range of 0.1%–100% at the frequencies of 1 Hz at 6 °C were performed to identify the linear viscoelastic region (LVR) of the hydrogel samples, followed by frequency sweeps from 0.1 to 100 rad s⁻¹ at a constant 1% strain. Shear rate sweeps in a range of 0.1–500 s⁻¹ were tested subsequently. The thixotropic property was investigated by exerting a shear rate at 0.1 s⁻¹ for 60 s (before printing) to the material, followed by increasing the shear rate to 100 s⁻¹ and maintained for 10 s (bio-inks being extruded through the needle tip causes the high shear rate), and finally, decreasing the shear rate to 0.1 s⁻¹ for 60 s (recovery). The viscosity over time was recorded.

Table 1. Composition of the samples and control groups and their corresponding labels.

	Samples	Control	
		Pure starch	Starch–collagen blend
Starch (S)	7.5%, 10%, 12.5%	7.5%, 10%, 12.5%	7.5%, 10%, 12.5%
Collagen (C)	1.33 mg mL ⁻¹	/	1.33 mg mL ⁻¹
GNP (G)	5×10 ⁹ , 10×10 ⁹	/	/
Sample formulations	7.5 S-1.33 C-5 G	7.5 S	7.5 S-1.33 C
	7.5 S-1.33 C-10 G	10 S	10 S-1.33 C
	10 S-1.33 C-5 G	12.5 S	12.5 S-1.33 C
	10 S-1.33 C-10 G		
	12.5 S-1.33 C-5 G		
	12.5 S-1.33 C-10 G		

Printing and Structural Integrity Evaluation: All the 3D bioprinting was performed with the EnvisionTEC 3D Bioplotter. Material was loaded into a sterile 30cc cartridge and extruded through a tapered 25G needle tip (ID = 260 μm). The temperature of the printing cartridge was maintained at 6 °C during printing. Printing pressure and speed were manually optimized for each combination. Each construct contains 10 layers. 15 mm \times 15 mm \times 2 mm scaffolds in grid pattern were printed directly into six-well culture plates. As proposed in the previous study,^[36] printability, which demonstrates the gelation of the bio-ink, could be calculated using the following equation:

$$Pr = \frac{L^2}{16A} \quad (2)$$

where L is the perimeter of the pore, A means the area of the pore. To obtain the Pr value of each bio-ink, optical images of printed constructs were captured and analyzed in Image-J software. The perimeter and area of the pores were achieved through threshold adjustment ($n = 4$). To demonstrate the printability of the selected bio-ink, a human anatomical ear shape was printed. The structural integrity of the nanoparticle/hydrogel composites in DPBS was examined for a consecutive 14 d. 3D printed rectangular samples (15 mm \times 15 mm \times 2 mm) were prepared as well. Samples were observed at various time intervals. The experiment was conducted ($N = 6$) under identical conditions.

Morphological Microstructure Characterization: Cryo-FE-SEM (CFE-SEM) was also used for visualizing and probing the pore structures, shapes, sizes, and content for a series of hydrogel composites: Starch, Starch-Collagen, Starch-Collagen-GNPs, and gelatin nanoparticles (GNPs). A 5 mm thick hydrogel (in the z-component) was flash-frozen within a tank of liquid nitrogen and immediately passed into the cryo-box attachment on the Hitachi FE-SEM. Fractionation within the cryo-box, by cleavage on the longitudinal plane, immediately proceeded and the sample was allowed to sublimate off the water under high negative pressure at 10^{-8} torr, analogous to lyophilization. Aperture and stigmata corrections were done before sample images were obtained. ImageJ was used to analyze the microstructures of the samples.

Cell Culture and Characterization: NIH 3T3 mouse fibroblasts (American Type Culture Collection, Manassas, VA) were cultured in DMEM supplemented with 10% FBS and 1% penicillin/streptomycin in a humidified incubator at 37 °C with 5% CO_2 . The cell culture medium was changed every 2–3 d, and the cells were harvested once they reached 80–90% confluence. Cells were labeled with cell tracker Red CMTPX for 30 min prior to seeding for the ease of visualization. For cell seeding, all the printed scaffolds were soaked in complete cell suspension for 3 h before seeding. Cells were then prepared with a density at 5×10^6 cells mL^{-1} , 40 μL cell suspension droplet was carefully placed onto the center of each scaffold surface, thereafter, the scaffold was incubated for 3–4 h in a CO_2 incubator to allow the cell attachment to the scaffolds. 1 mL medium was gently added to the culture well plate after the cells were attached. Medium was changed every day.

Similarly, cell metabolic activity was examined with the PrestoBlue assay. Samples ($n = 6$) were incubated with PrestoBlue at a ratio of 9:1 for 2 h at days 1, 4, and 7. To assess cell attachment and morphology, printed constructs were stained for phalloidin (F-actin in green) and 4',6-diamidino-2-phenylindole (DAPI; nuclei in blue) at days 4 and 7. Samples were fixed with 4% (v/v) paraformaldehyde for 30 min at room temperature, rinsed three times with PBS, then permeabilized with 0.2% (v/v) Triton X-100 for 30 min at room temperature. Afterward, the samples were thoroughly rinsed three times. Blocking buffer containing 5% bovine serum albumin (BSA) and 0.1% (v/v) Triton X-100 in PBS was added and incubated for 1 h. The samples were washed thrice after the removal of the blocking buffer. Alexa Fluor 488 Phalloidin (0.8 U mL^{-1}) and DAPI in PBS were added to each sample and incubated for 2 h and 30 min away from light to stain F-actin and nuclei, respectively.

The Cytation 5 Cell Imaging Multi-Mode Reader equipped with an inverted fluorescent microscope (widefield) was used for fluorescence cell imaging. Objectives with 4 \times and 20 \times magnifications were used. The fluorescence imaging channel was in the order of FITC followed

with DAPI. Images were processed by Gene 5 software with stitching function to achieve Figure 6a,b,e,f. The scaffold material has very light autofluorescence background which is much lower compared to fluorescence signals from labeled cells as shown in Figure S8 (Supporting Information). By applying image contrast, cells can be easily differentiated from scaffold materials and their stretching morphology was presented in Figure 6 and Figure S8 (Supporting Information).

Statistical Analysis: All results are expressed as mean value \pm standard deviation (SD) with a number of replicates indicated elsewhere in the Material and methods or in the figure captions. The results are evaluated by one-way ANOVA analysis coupled with a post-hoc Tukey test. Differences are considered statistically significant when $p \leq 0.05$ and greatly significant when $p \leq 0.001$.

Supporting Information

Supporting Information is available from the Wiley Online Library or from the author.

Acknowledgements

This project was supported by NIH NIGMS MIRA award 1R35GM133794 to Dr. Mei He.

Conflict of Interest

The authors declare no conflict of interest.

Data Availability Statement

The data that supports the findings of this study are available in the supplementary material of this article.

Keywords

3D bioprinting, collagen, nanoparticles, starch, tissue engineering

Received: May 8, 2021

Revised: July 21, 2021

Published online:

- [1] M. Askari, M. Afzali Naniz, M. Kouhi, A. Saberi, A. Zolfagharian, M. Bodaghi, *Biomater. Sci.* **2021**, 9, 535.
- [2] N. Liu, S. Huang, B. Yao, J. Xie, X. Wu, X. Fu, *Sci. Rep.* **2016**, 6, 34410.
- [3] P. Zhuang, J. An, C. K. Chua, L. P. Tan, *Mater. Des.* **2020**, 193, 108794.
- [4] R. Attalla, E. Puersten, N. Jain, P. R. Selvaganapathy, *Biofabrication* **2018**, 11, 15012.
- [5] J. Idaszek, M. Costantini, T. A. Karlsen, J. Jaroszewicz, C. Colosi, S. Testa, E. Fornetti, S. Bernardini, M. Seta, K. Kasarekto, R. Wrzesień, S. Cannata, A. Barbetta, C. Gargioli, J. E. Brinchman, W. Świąszkowski, *Biofabrication* **2019**, 11, 44101.
- [6] J. M. Unagolla, A. C. Jayasuriya, *Appl. Mater. Today* **2020**, 18, 100479.
- [7] P. Zhuang, A. X. Sun, J. An, C. K. Chua, S. Y. Chew, *Biomaterials* **2018**, 154, 113.
- [8] A. Schwab, R. Levato, M. D'Este, S. Piluso, D. Eglin, J. Malda, *Chem. Rev.* **2020**, 120, 11028.
- [9] Y. S. Zhang, A. Khademhosseini, *Science* **2017**, 356, eaaf3627.

- [10] E. O. Osidak, V. I. Kozhukhov, M. S. Osidak, S. P. Domogatsky, *Int. J. Bioprint.* **2020**, *6*, 270.
- [11] P. Zhuang, W. L. Ng, J. An, C. K. Chua, L. P. Tan, *PLoS One* **2019**, *14*, e0216776.
- [12] S. Zhang, D. Huang, H. Lin, Y. Xiao, X. Zhang, *Biomacromolecules* **2020**, *21*, 2400.
- [13] L. Ouyang, J. P. K. Armstrong, Y. Lin, J. P. Wojciechowski, C. Lee-Reeves, D. Hachim, K. Zhou, J. A. Burdick, M. M. Stevens, *Sci. Adv.* **2020**, *6*, eabc5529.
- [14] H. Chen, F. Xie, L. Chen, B. Zheng, *J. Food Eng.* **2019**, *244*, 150.
- [15] J. J. Perez, N. J. Francois, G. A. Maroniche, M. P. Borrajo, M. A. Pereyra, C. M. Creus, *Carbohydr. Polym.* **2018**, *202*, 409.
- [16] B. Amal, B. Veena, V. P. Jayachandran, J. Shilpa, *J. Mater. Sci.: Mater. Med.* **2015**, *26*, 181.
- [17] R. Shi, A. Zhu, D. Chen, X. Jiang, X. Xu, L. Zhang, W. Tian, *J. Appl. Polym. Sci.* **2010**, *115*, 346.
- [18] X. Wen, M. Shen, Y. Bai, C. Xu, X. Han, H. Yang, L. Yang, *J. Biomed. Mater. Res., Part B* **2020**, *108*, 104.
- [19] D. Wu, A. Samanta, R. K. Srivastava, M. Hakkarainen, *Biomacromolecules* **2017**, *18*, 1582.
- [20] F. Mirab, M. Eslamian, R. Bagheri, *Biomed. Phys. Eng. Express* **2018**, *4*, 55021.
- [21] A. Eskandarinia, A. Kefayat, M. Rafienia, M. Agheb, S. Navid, K. Ebrahimpour, *Carbohydr. Polym.* **2019**, *216*, 25.
- [22] F. G. Torres, S. Commeaux, O. P. Troncoso, *Starch/Staerke* **2013**, *65*, 543.
- [23] Y. Mao, M. Pan, H. Yang, X. Lin, L. Yang, *Front. Mater. Sci.* **2020**, *14*, 232.
- [24] V. S. Waghmare, P. R. Wadke, S. Dyawanapelly, A. Deshpande, R. Jain, P. Dandekar, *Bioact. Mater.* **2018**, *3*, 255.
- [25] H. M. Butler, E. Naseri, D. S. MacDonald, R. Andrew Tasker, A. Ahmadi, *Materialia* **2020**, *12*, 100737.
- [26] A. Nadernezhad, O. S. Caliskan, F. Topuz, F. Afghah, B. Erman, B. Koc, *ACS Appl. Bio Mater.* **2019**, *2*, 796.
- [27] S. A. Wilson, L. M. Cross, C. W. Peak, A. K. Gaharwar, *ACS Appl. Mater. Interfaces* **2017**, *9*, 43449.
- [28] S. Piluso, M. Labet, C. Zhou, J. W. Seo, W. Thielemans, J. Patterson, *Biomacromolecules* **2019**, *20*, 3819.
- [29] B. Begines, A. Alcudia, R. Aguilera-Velazquez, G. Martinez, Y. He, G. F. Trindade, R. Wildman, M.-J. Sayagues, A. Jimenez-Ruiz, R. Prado-Gotor, *Sci. Rep.* **2019**, *9*, 16097.
- [30] K. Behera, Y. H. Chang, M. Yadav, F. C. Chiu, *Polymer* **2020**, *186*, 122002.
- [31] Z. Cheng, L. Xigong, D. Weiye, H. Jingen, W. Shuo, L. Xiangjin, W. Junsong, *J. Nanobiotechnol.* **2020**, *18*, 97.
- [32] S. Ruan, X. Cao, X. Cun, G. Hu, Y. Zhou, Y. Zhang, L. Lu, Q. He, H. Gao, *Biomaterials* **2015**, *60*, 100.
- [33] B. Biduski, W. M. F. d. Silva, R. Colussi, S. L. d. M. E. Halal, L. T. Lim, Á.R. G. Dias, E. d. R. Zavareze, *Int. J. Biol. Macromol.* **2018**, *113*, 443.
- [34] S. Wang, C. Li, L. Copeland, Q. Niu, S. Wang, *Compr. Rev. Food Sci. Food Saf.* **2015**, *14*, 568.
- [35] J. A. Paten, S. M. Siadat, M. E. Susilo, E. N. Ismail, J. L. Stoner, J. P. Rothstein, J. W. Ruberti, *ACS Nano* **2016**, *10*, 5027.
- [36] L. Ouyang, R. Yao, Y. Zhao, W. Sun, *Biofabrication* **2016**, *8*, 35020.
- [37] W. Lim, S. Y. Shin, J. M. Cha, H. Bae, *Polymers* **2021**, *13*, 1773.
- [38] L. Ouyang, R. Yao, Y. Zhao, W. Sun, *Biofabrication* **2016**, *8*, 035020.
- [39] C. J. Coester, K. Langer, H. van Briesen, J. Kreuter, *J. Microencapsulation* **2000**, *17*, 187.
- [40] B. Burkel, B. A. Morris, S. M. Ponik, K. M. Riching, K. W. Eliceiri, P. J. Keely, *J. Visualized Exp.* **2016**, 53989.
- [41] S. KE, S. G, P. C, T. SM, E. KW, K. PJ, F. A, B. DJ, *Biomaterials* **2009**, *30*, 4833.

Q3

Reprint Order Form

Manuscript No.: _____

Customer No.: (if available) _____

Purchase Order No.: _____

Author: _____

Charges for Reprints in Euro (excl. VAT), prices are subject to change. Minimum order 50 copies.

No. of pages	50 copies	100 copies	150 copies	200 copies	300 copies	500 copies
1–4	345,—	395,—	425,—	445,—	548,—	752,—
5–8	490,—	573,—	608,—	636,—	784,—	1077,—
9–12	640,—	739,—	786,—	824,—	1016,—	1396,—
13–16	780,—	900,—	958,—	1004,—	1237,—	1701,—
17–20	930,—	1070,—	1138,—	1196,—	1489,—	2022,—
every additional 4 pages	147,—	169,—	175,—	188,—	231,—	315,—

Information regarding VAT: The charges for publication of *cover pictures /reprints/issues/poster/Video abstracts/* are considered to be “supply of services” and therefore subject to German VAT. However, if you are an institutional customer outside Germany, the tax can be waived if you provide us with the valid VAT number of your company. Non-EU customers may have a VAT number starting with “EU” instead of their country code, if they are registered with the EU tax authorities. If you do not have a valid EU VAT number and you are a taxable person doing business in a non-EU country, please provide a certification from your local tax authorities confirming that you are a taxable person under local tax law. Please note that the certification must confirm that you are a taxable person and are conducting an economic activity in your country. **Note:** certifications confirming that you are a tax-exempt legal body (non-profit organization, public body, school, political party, etc.) in your country do not exempt you from paying German VAT.

Please send me send bill me for

☐ no. of reprints

☐ high-resolution PDF file (330 Euro excl. VAT)

E-mail address: _____

❖ Special Offer:

If you order 200 or more reprints you will get a PDF file for half price.

Please note: It is not permitted to present the PDF file on the internet or on company homepages.

Cover Posters (prices excl. VAT)

Posters of published covers are available in two sizes:

☐ DinA2 42 x 60 cm / 17 x 24in (one copy: 39 Euro)

☐ DinA1 60 x 84 cm / 24 x 33in (one copy: 49 Euro)

Postage for shipping (prices excl. VAT)

overseas +25 Euro

within Europe +15 Euro

VAT number: _____

Mail reprints / copies of the issue to:

Send bill to:

☐ I will pay by bank transfer

☐ I will pay by credit card

VISA, Mastercard and AMERICAN EXPRESS

For your security please use this link (Credit Card Token Generator) to create a secure code Credit Card Token and include this number in the form instead of the credit card data. Click here:

https://www.wiley-vch.de/editorial_production/index.php

CREDIT CARD TOKEN NUMBER

						V													
--	--	--	--	--	--	---	--	--	--	--	--	--	--	--	--	--	--	--	--

Date, Signature _____